

Enhanced vapour sensing using silicon nanowire devices coated with Pt nanoparticle functionalized porous organic frameworks

Cao, Anping; Shan, Meixia; Paltrinieri, Laura; Evers, Wiel H.; Chu, Liangyong; Poltorak, Lukasz; Klootwijk, Johan H.; Seoane, Beatriz; Gascon, Jorge; Sudhölter, Ernst J.R.

DOI

[10.1039/c7nr07745a](https://doi.org/10.1039/c7nr07745a)

Publication date

2018

Document Version

Final published version

Published in

Nanoscale

Citation (APA)

Cao, A., Shan, M., Paltrinieri, L., Evers, W. H., Chu, L., Poltorak, L., Klootwijk, J. H., Seoane, B., Gascon, J., Sudhölter, E. J. R., & De Smet, L. C. P. M. (2018). Enhanced vapour sensing using silicon nanowire devices coated with Pt nanoparticle functionalized porous organic frameworks. *Nanoscale*, *10*(15), 6884-6891. <https://doi.org/10.1039/c7nr07745a>

Important note

To cite this publication, please use the final published version (if applicable).
Please check the document version above.

Copyright

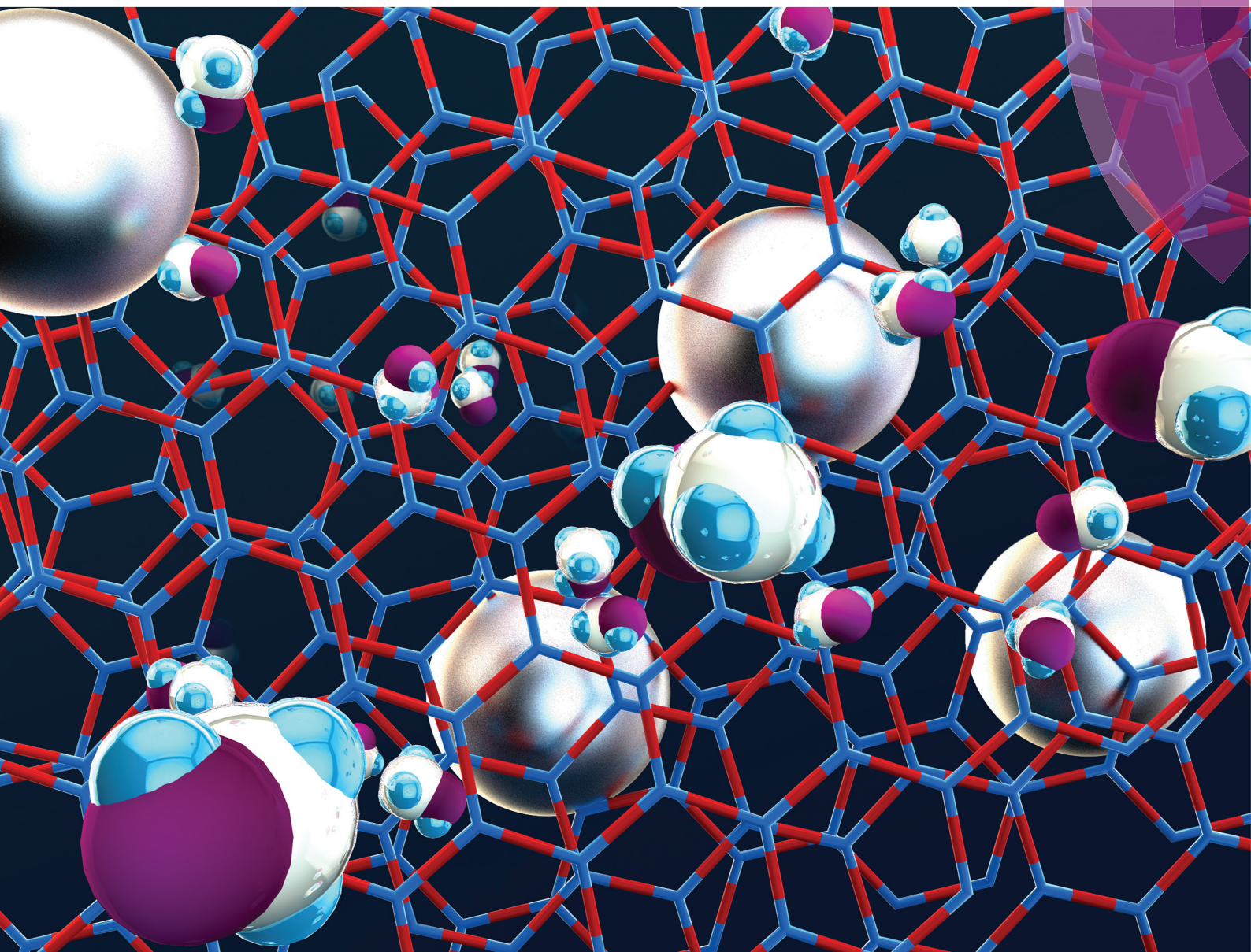
Other than for strictly personal use, it is not permitted to download, forward or distribute the text or part of it, without the consent of the author(s) and/or copyright holder(s), unless the work is under an open content license such as Creative Commons.

Takedown policy

Please contact us and provide details if you believe this document breaches copyrights.
We will remove access to the work immediately and investigate your claim.

Nanoscale

rsc.li/nanoscale



ISSN 2040-3372



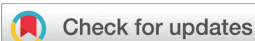
ROYAL SOCIETY
OF CHEMISTRY

PAPER

Louis C. P. M. de Smet *et al.*

Enhanced vapour sensing using silicon nanowire devices coated with Pt nanoparticle functionalized porous organic frameworks





Cite this: *Nanoscale*, 2018, **10**, 6884

Enhanced vapour sensing using silicon nanowire devices coated with Pt nanoparticle functionalized porous organic frameworks†

Anping Cao, ^{a,b} Meixia Shan,^a Laura Paltrinieri, ^{a,c} Wiel H. Evers, ^{a,d} Liangyong Chu, ^a Lukasz Poltorak, ^a Johan H. Klootwijk, ^e Beatriz Seoane, ^{a,f} Jorge Gascon, ^{a,g} Ernst J. R. Sudhölter ^a and Louis C. P. M. de Smet ^{*a,c,h}

Recently various porous organic frameworks (POFs, crystalline or amorphous materials) have been discovered, and used for a wide range of applications, including molecular separations and catalysis. Silicon nanowires (SiNWs) have been extensively studied for diverse applications, including as transistors, solar cells, lithium ion batteries and sensors. Here we demonstrate the functionalization of SiNW surfaces with POFs and explore its effect on the electrical sensing properties of SiNW-based devices. The surface modification by POFs was easily achieved by polycondensation on amine-modified SiNWs. Platinum nanoparticles were formed in these POFs by impregnation with chloroplatinic acid followed by chemical reduction. The final hybrid system showed highly enhanced sensitivity for methanol vapour detection. We envisage that the integration of SiNWs with POF selector layers, loaded with different metal nanoparticles will open up new avenues, not only in chemical and biosensing, but also in separations and catalysis.

Received 17th October 2017,
Accepted 23rd February 2018

DOI: 10.1039/c7nr07745a

rsc.li/nanoscale

Introduction

Improved sensitivity and selectivity in the detection of gas-phase molecules for environmental monitoring, process control and safety, and medical diagnosis is of utmost importance.¹ One promising approach for the direct electrical detection of analytes is by using nanowires configured as field-effect transistors (FETs), which exhibit superior sensitivity as given

by their high surface-to-volume ratio and the direct signal amplification by the transistor function.^{2,3} Particularly silicon nanowire-based FETs (SiNW-FETs), pioneered by Lieber's group,⁴ have been studied for more than 15 years now and have attracted a great deal of interest, mainly for their controllable properties and compatibility with very-large-scale integration (VLSI) processes and complementary metal-oxide-semiconductor (CMOS) technologies.^{5,6} While most SiNW-FET studies focus on detection of analytes in aqueous solutions,^{7,8} different gas-phase applications of electrical SiNW-based devices are attracting increasing interest.⁹ For instance, the research group of Haick published a number of systematic studies on the fundamentals and applications of functionalized SiNW-based FETs for the detection of volatile organic compounds (VOCs).^{10,11} In addition, surface functionalization of SiNWs with Pd nanoparticles,¹² oligopeptides,¹³ diphenylchlorophosphate (DPCP) receptors,¹⁴ or 3-aminopropyltrimethoxysilane (APTES)¹⁵ allowed for the rapid detection of H₂, acetic acid vapours, DPCP and explosives, respectively. All these studies have shown the advantages of controlled surface modification of the SiNWs in tuning sensor selectivity.

A variety of porous materials,¹⁶ such as metal organic polyhedra (MOPs),¹⁷ metal organic frameworks (MOFs)¹⁸ and covalent organic frameworks (COFs),¹⁹ have gained a lot of interest due to their exceptionally high specific surface areas, high specific gas storage and separation capabilities and their potential in catalysis and sensing applications,^{20,21} and other

^aDepartment of Chemical Engineering, Delft University of Technology, Delft, The Netherlands. E-mail: louis.desmet@wur.nl

^bStimuli-responsive Functional Materials and Devices, Department of Chemical Engineering and Chemistry, Eindhoven University of Technology, Eindhoven, The Netherlands

^cWetsus – European centre of excellence for sustainable water technology, Leeuwarden, The Netherlands

^dKavli Institute of Nanoscience, Delft University of Technology, Delft, The Netherlands

^ePhilips Research Laboratories, Eindhoven, The Netherlands

^fInorganic Chemistry and Catalysis group, Debye Institute for Nanomaterials Science, Utrecht University, Utrecht, The Netherlands

^gKing Abdullah University of Science and Technology, KAUST Catalysis Center, Advanced Catalytic Materials, Thuwal 23955, Saudi Arabia

^hLaboratory of Organic Chemistry, Wageningen University & Research, Wageningen, The Netherlands

† Electronic supplementary information (ESI) available: Surface functionalization; gas sorption analysis; X-ray photoelectron spectroscopy; ellipsometry; sensor fabrication and characterization; other measurements and results; the tomography of hybrid materials PtNP@POFs (TEM images were taken from different tilted angles) in MPG format. See DOI: 10.1039/c7nr07745a

electronic devices related to, *e.g.*, resistance-switching memory,²² high-performance dielectrics,²³ and proton conductivity.²⁴ The chemical diversity of these porous materials allows for a fine-tuning of the chemical and physical properties by tailored synthesis.²⁵ In addition, the exposure of properly designed affinity sites on the porous materials enable further coupling of functional substrates, for instance to Au plasmonic substrates and to SiNW platforms, expanding their application window significantly.^{20,26} Along these lines, we developed and explored a unique hybrid construct: porous organic framework (POF)-decorated SiNWs for the investigation of chemical vapour sensing. POFs are extremely attractive as affinity layers as they are not only highly porous, but also highly stable due to the formation of covalent bonds rather than metal coordination bonds; some of the early reported MOF structures decompose gradually if environmental moisture is present.²⁷ In addition, post-synthesis strategies can be applied to POFs to further tune their physico-chemical properties. We report here on a surface modification strategy to yield POF-functionalized, SiNW-based devices, after which the electrical properties of the resulting hybrid construct were investigated upon changes in the environmental humidity and methanol vapours. Moreover, the post-synthesis functionalization of the POF-SiNW hybrid by the *in situ* formation of Pt nanoparticles (PtNPs) results in advanced sensing properties of methanol vapours.

Results and discussion

The SiNW surface was functionalized with POFs *via* the polycondensation of melamine and terephthalaldehyde on the amine-modified SiNWs,²⁸ as illustrated in Fig. 1a and b. The POF-modified SiNWs together with the precipitated materials were harvested and cleaned for different characterizations.

The molecular details of the reactants and the effect of different solvents, temperature, reaction time and the use of

catalyst on the products were examined by Fourier Transform Infrared spectroscopy (FTIR), as shown in Fig. S1.† Only in the case of dimethyl sulfoxide (DMSO) as the solvent, the precipitate in the reaction solution was found to be flocculent. Reactions at the other conditions gave granular products. For the products obtained in all solvents the FTIR spectra show vibrations around 1550 cm⁻¹ and 1480 cm⁻¹, which are attributed to the stretching vibration of the triazine ring,²⁹ indicating the successful incorporation of the melamine into the molecular network. However, vibrations around 1690 cm⁻¹ (C=O stretching) are absent only for the product synthesized in DMSO, which proves that the highest conversion of functional groups initially present in the monomers was achieved in DMSO. Therefore, the reaction was optimized in this solvent. Moreover, the bands corresponding to imine bond vibration (*i.e.*, 1600 cm⁻¹) were absent in the FTIR spectra, indicating that the aldehyde group has reacted twice with an amino group from the melamine building block, forming aminal moieties. The high boiling point, combined with the high polarity of DMSO, contributes to the increased solubility of the initially formed polycondensated product *via* imine bonds, making subsequent condensations to aminal bonds possible as indicated by the structure in Fig. 1b.³⁰ In addition, considering the (in)stability of the Al electrodes on the SiNW chip during this reaction, we optimized the reaction time to 14 hours. Longer reaction times showed similar FTIR spectra of the product, as shown in Fig. S1b.†

The porous structure of the obtained flaky POF material synthesized under optimized conditions was investigated by N₂ gas sorption at 77 K (Fig. 2a). At low relative pressures a rapid uptake of N₂ is observed, indicating the presence of micropores. At high relative pressures (*i.e.*, $P/P_0 > 0.8$) some hysteresis is observed, which is attributed to the presence of mesopores where some capillary condensation can take place. At high relative pressures (*i.e.*, $P/P_0 > 0.9$) a steep rise in adsorption was observed, which indicates the presence of even larger pores, likely due to inter-particle porosity.³⁰ The calcu-

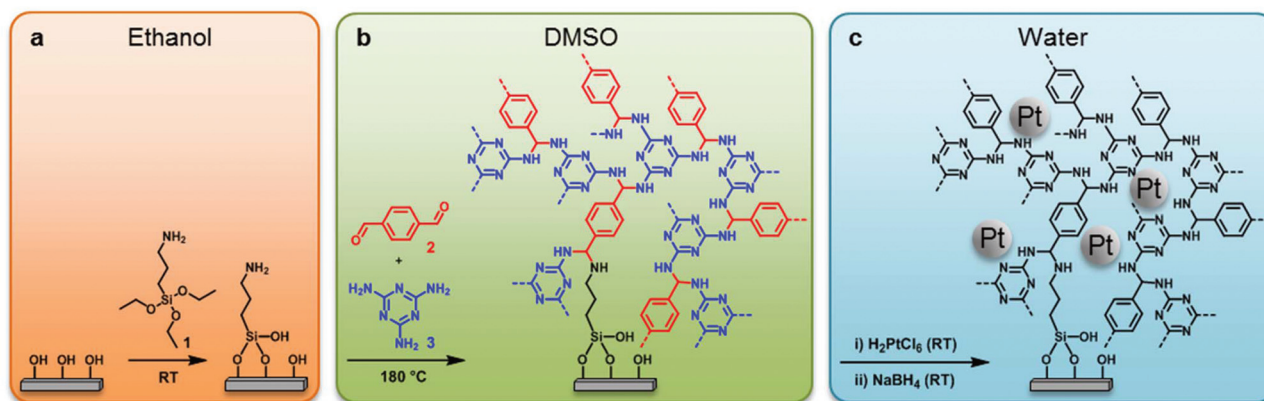


Fig. 1 Schematic representation of (a) APTES grafting to the silanol-terminated surface of a SiNW, (b) the covalent modification process of the SiNW surface with melamine-terephthalaldehyde-based POFs, (c) the metalation of a POF-SiNW *via* an *in situ* chemical reduction. Molecules 1–3: APTES, melamine, terephthalaldehyde, respectively.

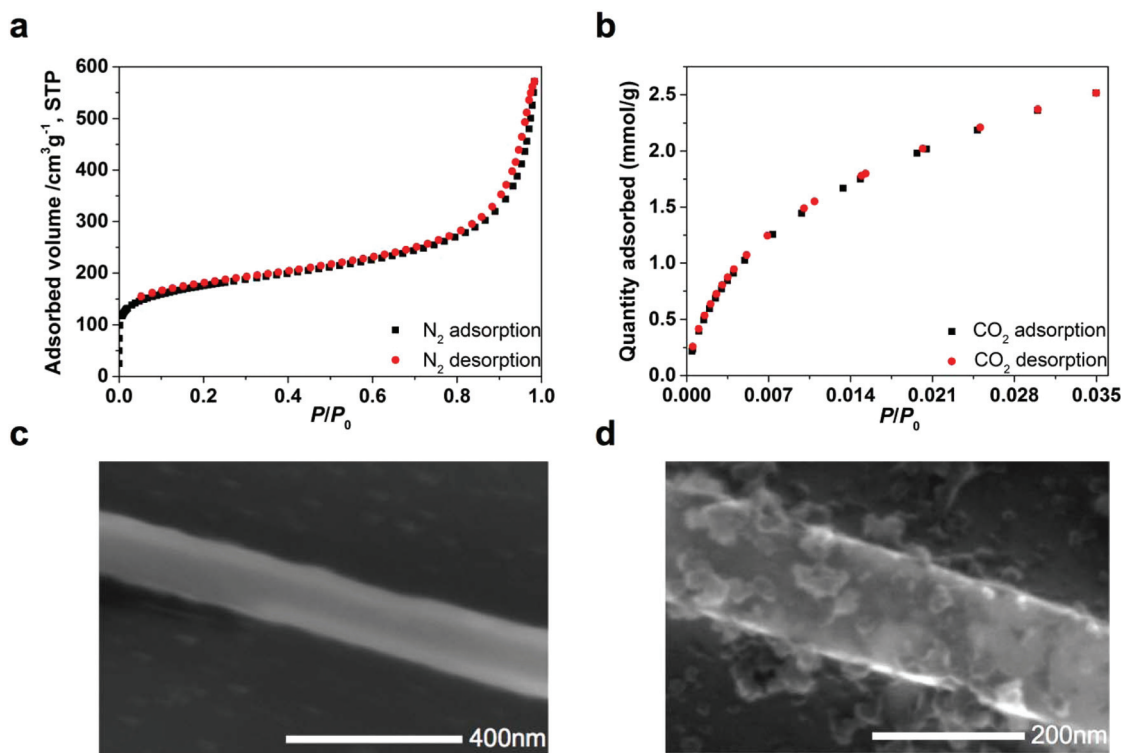


Fig. 2 (a) N_2 sorption isotherm acquired at 77 K, (b) CO_2 sorption isotherm acquired at 273 K of the POF powder synthesized under optimized conditions, (c) SEM image of the bare SiNW, (d) SEM image of the SiNW decorated with POFs.

lated Brunauer–Emmett–Teller (BET) specific surface area were found to be $620 \text{ m}^2 \text{ g}^{-1}$ and $640 \text{ m}^2 \text{ g}^{-1}$ for POFs synthesized for 14 hours and 72 hours, respectively. These values are lower than the one reported the first time for this material ($1377 \text{ m}^2 \text{ g}^{-1}$),²⁸ but very similar to more recently reported values for microporous organic polymer materials prepared *via* polycondensation (values ranging from 70 to $614 \text{ m}^2 \text{ g}^{-1}$).^{30–32} From the N_2 adsorption isotherms recorded at 77 K, the pore size distribution (PSD) was calculated with the use of Density Functional Theory (DFT), resulting in a pore diameter ranging from 1 to 55 nm (*i.e.*, micro- to mesopores; Fig. S2†).

Considering the presence of N atoms in the POF network and the likely favourable interaction with CO_2 , CO_2 sorption isotherms were measured up to 1.2 bar at 273 K (Fig. 2b). At 1 bar ($P/P_0 = 0.029$), the observed CO_2 uptake is 2.3 mmol g^{-1} , which is very similar to the high values of $\sim 2.0 \text{ mmol g}^{-1}$ and $\sim 1.5 \text{ mmol g}^{-1}$ as reported for the similar polymer networks (PI-1 and PI-2) rich in N atoms.³¹ The high value of CO_2 uptake here can be attributed to the high density of nitrogen in the POF structure originated from the melamine building blocks.

Similar surface modifications on silicon wafers were performed as model system for the SiNWs. These modified wafers were investigated by X-ray photoelectron spectroscopy (XPS) and compared with the unmodified wafers. The relative atomic surface composition of Si, O, C and N is shown in Table S1.† Upon modification with APTES, the N percentage increases

from 0 to 2.5%, indicating the successful silanization. Meanwhile, ellipsometry measurements showed 0.7 nm as the optical thickness, indicating a monolayer of APTES formed on the Si wafer.³³

After the POF polycondensation and POF coupling to the APTES layer, the N percentage increases to a value of 31%. The observed N/C ratio is found to be very similar to the ratio observed in the pure POF powder (31%). Inspection of the SiNW before and after surface modification by using scanning electron microscopy (SEM) showed the presence of flaky POF material on the nanowire (Fig. 2d). Similar flaky POF structures were observed on the modified silicon wafers (Fig. S3†).

Next, we have compared the electrical device response towards changes in humidity for POF-modified SiNWs and bare SiNWs using our home-built vapour sensing apparatus (Fig. S4†).^{34,35} Both types of p-doped SiNWs were set in the depletion mode by the application of a back-gate potential of $V_g = -3 \text{ V}$, and the varying drain–source current (I_{ds}) was registered under the conditions of a constant source–drain voltage (V_{ds}) set to 0.05 V. Step-wise increase of the relative humidity to RH = 46% shows for the bare SiNW a very slow increase of I_{ds} reaching more or less equilibrium after 2 h. The POF-modified SiNW showed a fast increase of I_{ds} and equilibration after *ca.* 3 min, which is around 40 times faster as compared to the unmodified sensor. The I_{ds} at equilibrium for the POF-modified SiNWs is about two times higher than for the bare SiNWs. In both situations the I_{ds} increases, indicating an increase of

the concentration of the majority charge carriers (here holes). This is understood as the injection of water vapour results in partial deprotonation of surface silanol groups on the SiNW and changes the surface charge from neutral to negative, as $\text{Si-OH} \rightleftharpoons \text{Si-O}^- + \text{H}^+$, ($\text{p}K_{\text{a}} \sim 4$).³⁶ The resulting negatively charged Si-O^- on the surface will bend the SiNW valence band up, leading to more holes flowing through the p-doped SiNW channel, thus explaining the observed increase of I_{ds} . For the POF-modified SiNWs this effect is enhanced both in time and in overall drain–source current effect. This is attributed to the presence of the flaky POF structure with its high specific surface area and its richness in N atoms. The high specific surface area will contribute to a fast and increased uptake of water into the porous structure, resulting in a pre-concentration effect. The water ($\text{p}K_{\text{a}} \sim 15.7$)³⁷ taken up and the present secondary amines (the most basic nitrogen present in the system with a $\text{p}K_{\text{a}}$ of 11,³⁷ while the $\text{p}K_{\text{a}}$ of melamine is ~ 5)³⁸ in the POF will facilitate the formation of ammonium derivatives and hydroxyl groups, contributing to the partial deprotonation of the silanol groups on the surface. The POF-modified SiNWs were also investigated with varying RH between 6 and 60% and I_{ds} was found to increase with RH (Fig. 3b).

The sensitivity responses for humidity variation of the POF-modified SiNW sensor are found to be very high; within the concentration range studied, the signal increased by ~ 2 orders of magnitude, which is comparable to the values reported for humidity sensors using nanoporous polymer membranes³⁹ and graphene oxide.⁴⁰ In addition, the POF-modified sensor showed a satisfactory level of repeatability towards water vapour sensing, as it is demonstrated in Fig. S5†

Given the high CO_2 uptake of the POF powder, we tested the CO_2 sensing using POF-modified SiNWs. However, varying amounts of CO_2 in N_2 in the range of 0.5–5% at room temperature and 1 bar in the presence of water (and without water) did not show any sensor response. We speculate that in a dry state at room temperature, CO_2 may interact with POFs through

physisorption. In such a case no ions are formed and therefore it hardly will affect the electrical properties of SiNWs. While primary/secondary amines, as well as triazine, can form carbamates with CO_2 ,^{41,42} we consider chemisorption to be unlikely, as the CO_2 isotherm in Fig. 2b shows hardly any adsorption–desorption hysteresis, suggesting a completely reversible physical adsorption in our system. For a wet state, CO_2 reacted with water and carbonic acid was formed, however, a clear change of pH was absent, therefore the water sensing dominates the outcome.

To further explore the application of POF-modified SiNWs, we studied the post-synthesis functionalization of the porous layer through Pt metalation. This functionalization strategy started with impregnating the POF material with an aqueous chloroplatinic acid solution (H_2PtCl_6), followed by a reduction step using sodium borohydride (NaBH_4), as illustrated in Fig. 1c. The chloroplatinic acid protonates the nitrogen sites in the POF to ammonium groups having the negatively charged $[\text{HPtCl}_6]^-$ as the counter ion. A suspension of POF in H_2PtCl_6 aqueous solution was shaken for different time intervals and the UV-vis absorption spectrum of the supernatant was recorded (Fig. S6a†). A clear decrease of the H_2PtCl_6 absorption at 259 nm in time is observed, indicating the adsorption of the metal precursor in the POF precipitate. After the metalation, the POF changed colour from off-white to yellow (Fig. S6b†). Subsequently, this material was treated with NaBH_4 , and a clear colour change from yellow to dark brown was observed for the POF material, indicating that the *in situ* reduction to metallic Pt has taken place.

Next, the sample was inspected by transmission electron microscopy (TEM). Clear Pt nanoparticles of *ca.* 2 nm in diameter were observed, well dispersed over the flaky polymeric organic framework (Fig. 4b, $\text{H}_2\text{PtCl}_6 : \text{N}$ in POF = 1 : 37). In the TEM image recorded before the reduction step, no nanoparticles were observed and the images are similar to the untreated POFs (Fig. S7†). Varying molar ratios of $\text{H}_2\text{PtCl}_6 : \text{N}$

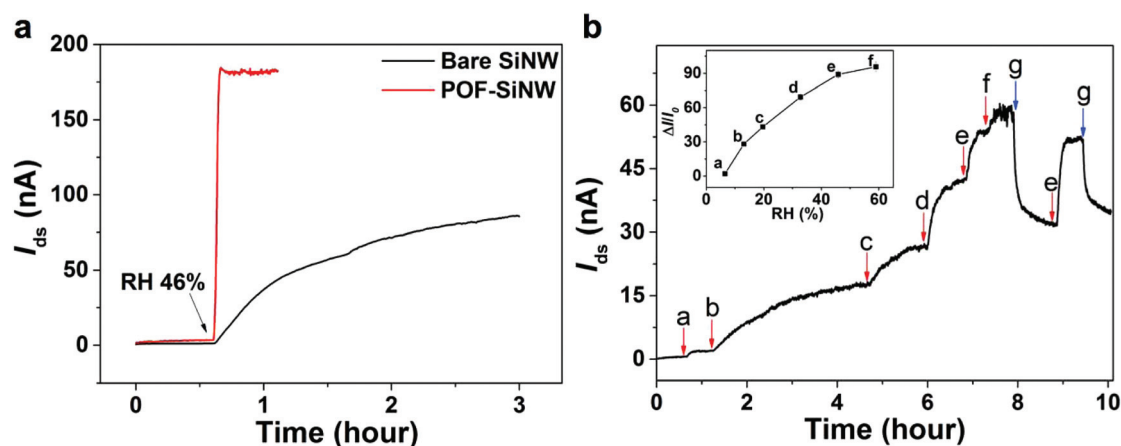


Fig. 3 Variation of drain–source current (I_{ds}) of a bare SiNW and a POF-modified SiNW with humidity at $V_{\text{g}} = -3$ V and $V_{\text{ds}} = 0.05$ V, (a) real-time variation of I_{ds} after a step-wise increase of the relative humidity from 0 to 46%, (b) increase of I_{ds} in time after the successive increase of RH from 0 to 60% (labels a–f refer to the injection of RH in 6.5, 13, 20, 33, 46 and 60%, respectively, while label g indicates the start of a pure N_2 flow). The inset shows the relative increase of I_{ds} as function of RH.

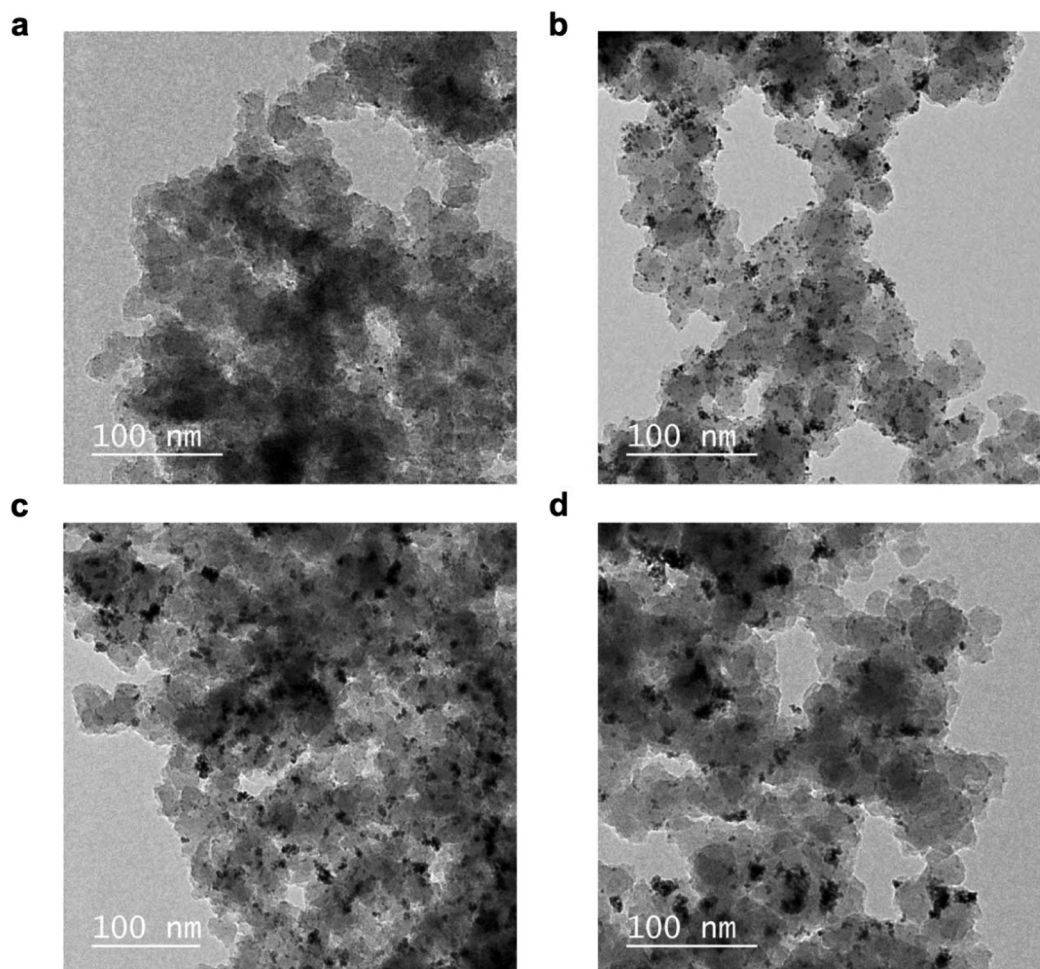


Fig. 4 TEM images after NaBH_4 reduction of POFs containing different amounts of H_2PtCl_6 , showing the formed Pt nanoparticles with different particle sizes. The molar ratios between H_2PtCl_6 and N atoms in the POFs are (a) 1 : 100, (b) 1 : 37, (c) 1 : 20, and (d) 1 : 4.

in POF have been investigated further: 1 : 100, 1 : 20, and finally 1 : 4 (Fig. 4a, c, and d, respectively). Upon increasing Pt : N ratio the single particle diameter was found to increase to 3–4 nm (Fig. 4c) and for the highest ratios also the presence of agglomerates is observed (Fig. 4d). To get a better insight in the tomography of the hybrid materials, TEM images were taken from different tilted angles, from which a 3D representation was reconstructed (ESI Movie 1†). From these results it can be seen that the formed Pt nanoparticles and agglomerates are found predominantly at the outer surface of the POF material and hardly inside the porous structure. This can be rationalized by a NaBH_4 reduction process that starts at the outside, resulting in the formation of Pt nanoparticles that block further entrance of the reducing agent into the porous structure. Table S2† summarizes the textural properties and CO_2 uptake of the metalized POFs with different molar ratios of H_2PtCl_6 : N in the POF, nicely showing that the BET surface, micropore volume and CO_2 uptake decreased for increasing amounts of PtNPs.

To verify the metalation of POF and further *in situ* reduction taken place on POF-modified Si substrate, XPS analysis was

conducted. Fig. 5a (powder sample) and Fig. 5c (modified Si wafer) show high-resolution region spectra of Pt 4f of the metalation of the products before the reduction. Both spectra show two main peaks at 73.2 eV and 76.8 eV, corresponding to Pt 4f_{7/2} and 4f_{5/2} of PtCl_4^{2-} species, respectively.⁴³ After the NaBH_4 reduction, two peaks at 71.5 eV and 74.7 eV, corresponding to Pt⁰ 4f_{7/2} and 4f_{5/2}, respectively, are much more prominent in the spectra (Fig. 5b and d), which indicates the anchored Pt species are predominantly in the metallic state.

The method for the successful POF impregnation with H_2PtCl_6 and the subsequent chemical reduction to metallic Pt nanoparticles has also been applied to POF-decorated SiNWs, to see whether this would have an effect on the affinity properties of the sensor coating. We first investigated the electrical behaviour of PtNP@POF-functionalised SiNWs to varying methanol vapour concentrations in the range of 1200 to 6400 ppm. Under the same depletion-mode conditions as described before the change of I_{ds} was monitored. Increasing the methanol vapour concentration results in an increase of I_{ds} (Fig. 6a). From the comparison with the response observed for the bare SiNW (which showed hardly any response) and the

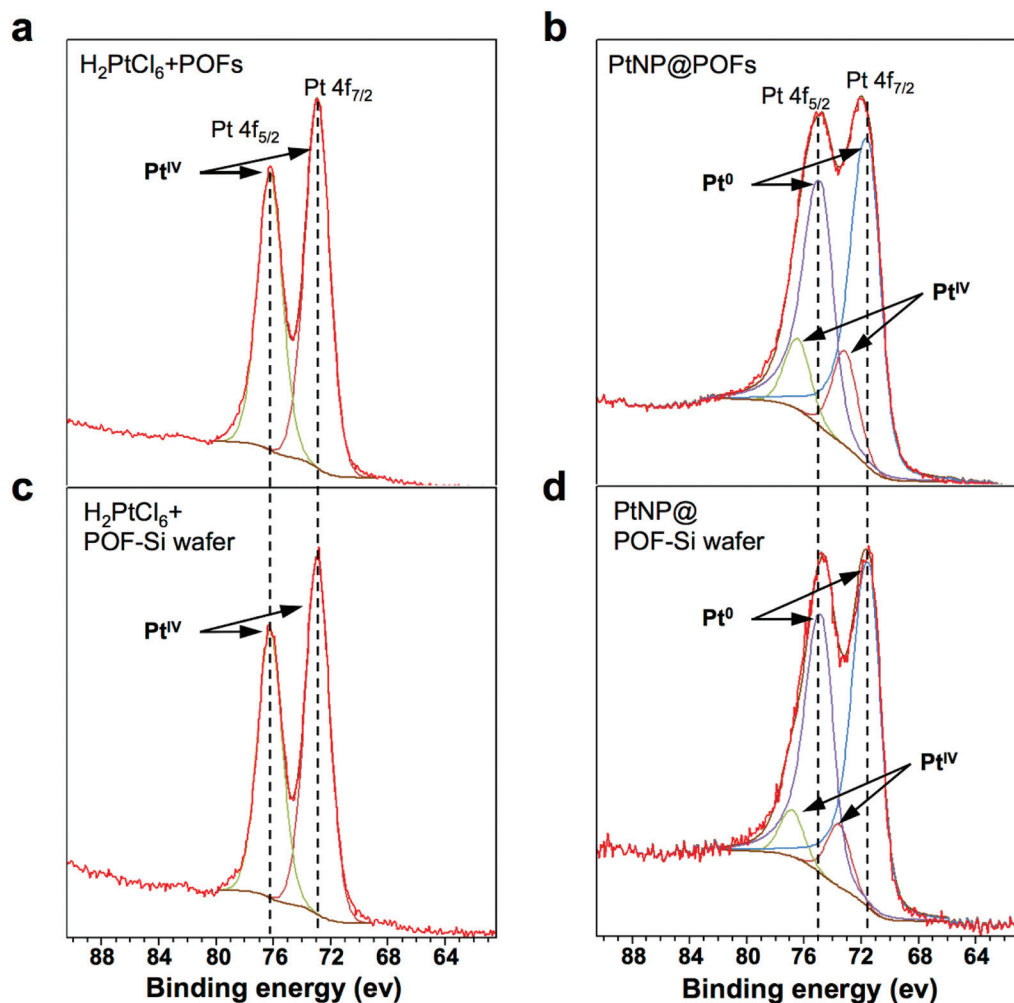


Fig. 5 Pt 4f XPS region spectra of samples related to the (a) metalation of POF powder, (b) metalation of POF powder after reduction, (c) metalation of POF-Si wafer, (d) metalation of POF-Si wafer after reduction.

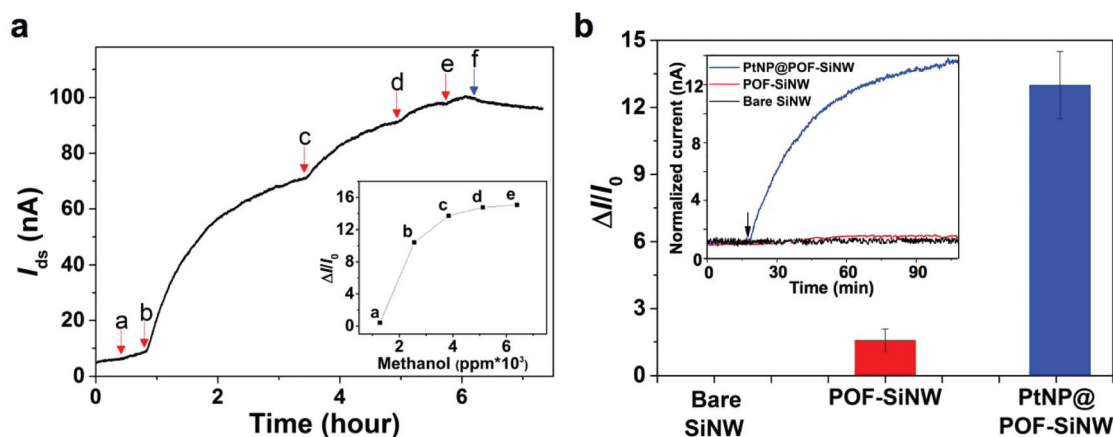


Fig. 6 (a) Increase of I_{ds} as function of time after the successive increase of the methanol vapour concentration from 1200 to 6400 ppm of PtNP@POF-SiNW devices (labels a–e represent the moment of the injection of methanol vapour concentration at 1200, 2500, 3800, 5100, and 6400 ppm, and label f represents the moment of injecting a pure N_2 flow) at $V_g = -3$ V and $V_{ds} = 0.05$ V. The inset shows the relative increase of I_{ds} ($\Delta I/I_0$) as function of the methanol vapour concentration. (b) Normalized response upon exposure to 3000 ppm of methanol vapour for bare SiNW, POF-SiNW and PtNP@POF-SiNW sensors.

POF-SiNW (response increase of *ca.* 150%; Fig. 6b), the enhanced effect of the Pt nanoparticles on the methanol response becomes very clear (increase of response of *ca.* 1350%). These results can be interpreted as follows. For the bare SiNW the injection of methanol vapour with the indicated concentration was not sufficient to affect the silanol dissociation; a similar performance has been reported by others.⁴⁴ For the POF-SiNW the injection of methanol showed an increase in response. As explained earlier for water, we attribute this to a pre-concentration effect. Although methanol is a slightly weaker acid than water ($pK_a \sim 16$ vs. 15.7)³⁷ it can protonate the secondary amines of the POFs as well, leaving the methoxide ions to dissociate the silanol groups, inducing a (more) negative surface charge, increasing the current of the p-type SiNW. For the PtNP@POF-SiNWs, the observed enhanced response toward methanol vapour, indicates an even higher methanol pre-concentration due to the presence of PtNPs. The observed increase in response upon the incorporation of Pt(0) NPs in the POF is directly related to an enhanced dissociation of the surface silanol groups of the SiNW, which may be explained by an increased amount of base (here methoxide ions) present in the system. This is only possible by an increased basicity of the Pt(0)NP@POF compared to the pure POF, which can be attributed to an increased basicity of the secondary nitrogens present in the POF. This could be, *e.g.*, due to a net charge transfer from Pt(0) to these nitrogens, comparable to charge transfers reported in other Pt–N interactions.^{45,46} Also, the enhancement could be the result of the improved sensitivity of the device due to the capacitive coupling of the gate potential *via* these PtNPs to the SiNW.⁴⁷ This implies that the potential of the PtNPs follows the back-gate potential, which contributes to the accumulation of holes in the SiNW channel near the PtNP sites. Similar results have been observed for PdNP-decorated SiNWs and SiNW biosensors.^{47–49}

Lastly, cross-reactivity of the PtNP@POF-SiNW devices to other structurally related VOCs was also investigated (Fig. S8†). The results clearly show the highest response for methanol vapour, over ethanol, isopropanol and acetaldehyde vapours. This trend follows the one of the dielectrical constants ($\epsilon_r = 33, 24.5, 21.1, 16.5$, for these analytes, respectively);³⁷ the higher ϵ_r the higher the polarity and the more favourable to the dissociation of Si–O \cdots H–B $^-$ ion pair (where B $^-$ stands for the base) to Si–O $^-$ and HB.

Conclusions

In this study, POFs have been successfully covalently coupled to APTES-modified SiNWs. The observed increased sensitivity for water vapour detection, compared to the unmodified SiNW, is attributed to the enhanced water affinity by the high surface area of POFs, resulting in an increased surface silanol dissociation and concomitant increase of majority charge carriers (holes) and therefore an increase of the I_{ds} . Post-synthesis modification of the POFs results in the formation of well-dis-

persed and size-controlled PtNPs. The presence of the PtNPs in the POF contributes to the observed enhanced sensitivity for the detection of methanol vapour, likely as a consequence of the pre-concentration of methanol vapour and the capacitive coupling of the gate potential *via* the PtNPs to the SiNW. This study presents a synthetic strategy that is expected to be applicable to other post-synthesis (surface) modifications using a range of metal precursors. The resulting hybrid systems might find utilization not only in chemical and (bio)sensing, but also in gas separations and catalysis.

Conflicts of interest

There are no conflicts to declare.

Acknowledgements

The authors thank NanoNextNL, a micro and nanotechnology consortium of the Government of The Netherlands and 130 partners, for their financial support. Laura P. and L. C. P. M. d. S. thank Wetsus – European centre of excellence for sustainable water technology for funding. M. S. and L. C. thank the China Scholarship Council (CSC) for financial support. L. C. P. M. d. S. acknowledges the European Research Council (ERC) for a Consolidator Grant, which is part of the European Union's Horizon 2020 research and innovation programme (grant agreement no 682444). We also thank Mr Duco Bosma and Mr Bart Boshuizen from TU Delft for technical and LabVIEW support and Mr Tiny Verhoeven (TU Eindhoven) for performing some of the XPS measurements.

References

- 1 A. Tricoli, M. Righettoni and A. Teleki, *Angew. Chem., Int. Ed.*, 2010, **49**, 7632–7659.
- 2 B. L. Allen, P. D. Kichambare and A. Star, *Adv. Mater.*, 2007, **19**, 1439–1451.
- 3 G. T. Chandran, X. Li, A. Ogata and R. M. Penner, *Anal. Chem.*, 2017, **89**, 249–275.
- 4 Y. Cui and C. M. Lieber, *Science*, 2001, **291**, 851–853.
- 5 E. Stern, J. F. Klemic, D. A. Routenberg, P. N. Wyrembak, D. B. Turner-Evans, A. D. Hamilton, D. A. LaVan, T. M. Fahmy and M. A. Reed, *Nature*, 2007, **445**, 519–522.
- 6 M. Mescher, L. C. P. M. de Smet, E. J. R. Sudhölter and J. H. Klootwijk, *J. Nanosci. Nanotechnol.*, 2013, **13**, 5649–5653.
- 7 X. Duan, Y. Li, N. K. Rajan, D. A. Routenberg, Y. Modis and M. A. Reed, *Nat. Nanotechnol.*, 2012, **7**, 401–407.
- 8 T. E. Bae, H. J. Jang, J. H. Yang and W. J. Cho, *ACS Appl. Mater. Interfaces*, 2013, **5**, 5214–5218.
- 9 A. Cao, E. J. R. Sudhölter and L. C. P. M. de Smet, *Sensors*, 2014, **14**, 245–271.
- 10 Y. Paska, T. Stelzner, S. Christiansen and H. Haick, *ACS Nano*, 2011, **5**, 5620–5626.

- 11 Y. Paska, T. Stelzner, O. Assad, U. Tisch, S. Christiansen and H. Haick, *ACS Nano*, 2012, **6**, 335–345.
- 12 Z. H. Chen, J. S. Jie, L. B. Luo, H. Wang, C. S. Lee and S. T. Lee, *Nanotechnology*, 2007, **18**, 345502.
- 13 M. C. McAlpine, H. D. Agnew, R. D. Rohde, M. Blanco, H. Ahmad, A. D. Stuparu, W. A. Goddard and J. R. Heath, *J. Am. Chem. Soc.*, 2008, **130**, 9583–9589.
- 14 S. Clavaguera, A. Carella, L. Caillier, C. Celle, J. Pecaut, S. Lenfant, D. Vuillaume and J. P. Simonato, *Angew. Chem., Int. Ed.*, 2010, **49**, 4063–4066.
- 15 Y. Engel, R. Elnathan, A. Pevzner, G. Davidi, E. Flaxer and F. Patolsky, *Angew. Chem., Int. Ed.*, 2010, **49**, 6830–6835.
- 16 A. G. Slater and A. I. Cooper, *Science*, 2015, **348**, aaa8075.
- 17 H. Vardhan, M. Yusubov and F. Verpoort, *Coord. Chem. Rev.*, 2016, **306**, 171–194.
- 18 H. Furukawa, K. E. Cordova, M. O’Keeffe and O. M. Yaghi, *Science*, 2013, **341**, 1230444.
- 19 X. Feng, X. Ding and D. Jiang, *Chem. Soc. Rev.*, 2012, **41**, 6010–6022.
- 20 C. Wang, J. Shang, Y. Lan, T. Tian, H. Wang, X. Chen, J. Y. Gu, J. Z. Liu, L. J. Wan, W. Zhu and G. Li, *Adv. Funct. Mater.*, 2015, **25**, 6009–6017.
- 21 I. Stassen, N. Burtch, A. Talin, P. Falcaro, M. Allendorf and R. Ameloot, *Chem. Soc. Rev.*, 2017, **46**, 3185–3241.
- 22 Y. Liu, H. Wang, W. Shi, W. Zhang, J. Yu, B. K. Chandran, C. Cui, B. Zhu, Z. Liu, B. Li, C. Xu, Z. Xu, S. Li, W. Huang, F. Huo and X. Chen, *Angew. Chem., Int. Ed.*, 2016, **55**, 8884–8888.
- 23 W. J. Li, J. Liu, Z. H. Sun, T. F. Liu, J. Lü, S. Y. Gao, C. He, R. Cao and J. H. Luo, *Nat. Commun.*, 2016, **7**, 11830.
- 24 H. Ma, B. Liu, B. Li, L. Zhang, Y. G. Li, H. Q. Tan, H. Y. Zang and G. Zhu, *J. Am. Chem. Soc.*, 2016, **138**, 5897–5903.
- 25 S. Das, P. Heasman, T. Ben and S. Qiu, *Chem. Rev.*, 2017, **117**, 1515–1563.
- 26 A. Cao, W. Zhu, J. Shang, J. H. Klootwijk, E. J. R. Sudhölter, J. Huskens and L. C. P. M. de Smet, *Nano Lett.*, 2017, **17**, 1–7.
- 27 C. Wang, X. Liu, N. Keser Demir, J. P. Chen and K. Li, *Chem. Soc. Rev.*, 2016, **45**, 5107–5134.
- 28 M. G. Schwab, B. Fassbender, H. W. Spiess, A. Thomas, X. L. Feng and K. Mullen, *J. Am. Chem. Soc.*, 2009, **131**, 7216–7217.
- 29 N. E. Mircescu, M. Oltean, V. Chis and N. Leopold, *Vib. Spectrosc.*, 2012, **62**, 165–171.
- 30 C. Xu and N. Hedin, *J. Mater. Chem. A*, 2013, **1**, 3406–3414.
- 31 A. Laybourn, R. Dawson, R. Clowes, J. A. Iggo, A. I. Cooper, Y. Z. Khimiyak and D. J. Adams, *Polym. Chem.*, 2012, **3**, 533–537.
- 32 B. P. Biswal, S. Chandra, S. Kandambeth, B. Lukose, T. Heine and R. Banerjee, *J. Am. Chem. Soc.*, 2013, **135**, 5328–5331.
- 33 M. J. Zhu, M. Z. Lerum and W. Chen, *Langmuir*, 2012, **28**, 416–423.
- 34 S. Sachdeva, S. J. H. Koper, A. Sabetghadam, D. Socco, D. J. Gravesteijn, F. Kapteijn, E. J. R. Sudhölter, J. Gascon and L. C. P. M. de Smet, *ACS Appl. Mater. Interfaces*, 2017, **9**, 24926–24935.
- 35 S. Sachdeva, M. R. Venkatesh, B. El Mansouri, J. Wei, A. Bossche, F. Kapteijn, G. Q. Zhang, J. Gascon, L. C. P. M. de Smet and E. J. R. Sudhölter, *Small*, 2017, **13**, 1604150.
- 36 K. Leung, I. M. B. Nielsen and L. J. Criscenti, *J. Am. Chem. Soc.*, 2009, **131**, 18358–18365.
- 37 M. B. Smith and J. March, *March’s advanced organic chemistry: reactions, mechanisms, and structure*, John Wiley & Sons, New York, 2001, 7th edn.
- 38 Dissociation Constants of Organic Acids and Bases, https://labs.chem.ucsb.edu/zhang/liming/pdf/pKas_of_Organic_Acids_and_Bases.pdf, (accessed September 2017).
- 39 B. Yang, B. Aksak, Q. Lin and M. Sitti, *Sens. Actuators, B*, 2006, **114**, 254–262.
- 40 S. Borini, R. White, D. Wei, M. Astley, S. Haque, E. Spigone, N. Harris, J. Kivioja and T. Ryhanen, *ACS Nano*, 2013, **7**, 11166–11173.
- 41 E. A. Prasetyanto, M. B. Ansari, B.-H. Min and S.-E. Park, *Catal. Today*, 2010, **158**, 252–257.
- 42 A. Goepfert, M. Czaun, R. B. May, G. K. S. Prakash, G. A. Olah and S. R. Narayanan, *J. Am. Chem. Soc.*, 2011, **133**, 20164–20167.
- 43 R. Fu, H. Zeng, Y. Lu, S. Y. Lai, W. H. Chan and C. F. Ng, *Carbon*, 1995, **33**, 657–661.
- 44 A. O. Niskanen, A. Colli, R. White, H. W. Li, E. Spigone and J. M. Kivioja, *Nanotechnology*, 2011, **22**, 295502.
- 45 J. Ma, A. Habrioux, Y. Luo, G. Ramos-Sanchez, L. Calvillo, G. Granozzi, P. B. Balbuena and N. Alonso-Vante, *J. Mater. Chem. A*, 2015, **3**, 11891–11904.
- 46 E. Gracia-Espino, X. Jia and T. Wågberg, *J. Phys. Chem. C*, 2014, **118**, 2804–2811.
- 47 B. Choi, J. H. Ahn, J. Lee, J. Yoon, J. Lee, M. Jeon, D. M. Kim, D. H. Kim, I. Park and S. J. Choi, *Solid-State Electron.*, 2015, **114**, 76–79.
- 48 H. Jang, J. Lee, J. H. Lee, S. Seo, B.-G. Park, D. M. Kim, D. H. Kim and I.-Y. Chung, *Appl. Phys. Lett.*, 2011, **99**, 252103.
- 49 S. Pud, J. Li, V. Sibiliev, M. Petrychuk, V. Kovalenko, A. Offenhäusser and S. Vitusevich, *Nano Lett.*, 2014, **14**, 578–584.